Plio-Pleistocene glacial-interglacial productivity changes in the eastern equatorial Pacific upwelling system

Kim Jakob, Paul A. Wilson, André Bahr, Clara T. Bolton, Jörg Pross, Jens Fiebig, Oliver Friedrich

AGU PUBLICATIONS

Paleoceanography

RESEARCH ARTICLE
10.1002/2015PA002899

Key Points:
- Maximum in export production was reached toward glacial terminations
- Enhanced nutrient delivery from high southern latitudes during full glacial conditions
- Equatorial upwelling intensification toward glacial terminations

Supporting Information:
- Supporting Information S1
- Data Set S1

Correspondence to:
K. A. Jakob,
kim.jakob@geow.uni-heidelberg.de

Citation:
Jakob, K. A., P. A. Wilson, A. Bahr, C. T. Bolton, J. Pross, J. Fiebig, and O. Friedrich (2016), Plio-Pleistocene glacial-interglacial productivity changes in the eastern equatorial Pacific upwelling system, *Paleoceanography*, *31*, 453–470, doi:10.1002/2015PA002899.

Received 10 NOV 2015
Accepted 2 MAR 2016
Accepted article online 9 MAR 2016
Published online 24 MAR 2016

Plio-Pleistocene glacial-interglacial productivity changes in the eastern equatorial Pacific upwelling system

Kim A. Jakob[1], Paul A. Wilson[2], André Bahr[1], Clara T. Bolton[3], Jörg Pross[1], Jens Fiebig[4], and Oliver Friedrich[1]

[1]Institute of Earth Sciences, Heidelberg University, Heidelberg, Germany, [2]National Oceanography Centre Southampton, University of Southampton, Southampton, UK, [3]Aix-Marseille Université, CNRS, IRD, CEREGE UM 34, Aix-en-Provence, France, [4]Institute of Geosciences, Goethe University Frankfurt, Frankfurt, Germany

Abstract The eastern equatorial Pacific Ocean (EEP) upwelling system supports >10% of the present-day global ocean primary production, making it an important component in Earth's atmospheric and marine carbon budget. Traditionally, it has been argued that since intensification of Northern Hemisphere glaciation (iNHG, ~2.7 Ma), changes in EEP productivity have predominantly depended on trade wind strength-controlled upwelling intensity. An alternative hypothesis suggests that EEP productivity is primarily controlled by nutrient supply from the high southern latitudes via mode waters. Here we present new high-resolution data for the latest Pliocene/early Pleistocene from Ocean Drilling Program Site 849, located within the equatorial divergence system in the heart of the EEP upwelling regime. We use carbon isotopes in benthic and planktic foraminiferal calcite and sand accumulation rates to investigate glacial-interglacial (G-IG) productivity fluctuations between 2.65 and 2.4 Ma (marine isotope stages (MIS) G1 to 94). This interval includes MIS 100, 98, and 96, three large-amplitude glacials (~1‰ in benthic $\delta^{18}O$) representing the culmination of iNHG. Our results suggest that latest Pliocene/early Pleistocene G-IG productivity changes in the EEP were strongly controlled by nutrient supply from Southern Ocean-sourced mode waters. Our records show a clear G-IG cyclicity from MIS 100 onward with productivity levels increasing from full glacial conditions and peaking at glacial terminations. We conclude that enhanced nutrient delivery from high southern latitudes during full glacial conditions together with superimposed intensified regional upwelling toward glacial terminations strongly regulated primary productivity rates in the EEP from MIS 100 onward.

1. Introduction

Oceanic upwelling regions play a key role in controlling Earth's climate [e.g., *Toggweiler and Sarmiento*, 1985; *Watson and Garabato*, 2006]. High phytoplankton growth rates and standing stocks supported by relatively nutrient-rich waters in upwelling zones promote organic matter export from the surface ocean and removal of CO_2 from the surface ocean-atmosphere system [e.g., *Schlitzer*, 2004; *Takahashi et al.*, 2009], with a significant influence on both the global carbon and nutrient cycles [e.g., *Schlitzer*, 2004]. An ideal natural laboratory for studying the dynamics of an upwelling system is the eastern equatorial Pacific Ocean (EEP). There, both equatorial upwelling and coastal upwelling contribute to conditions that support more than 10% of the global biological production in the present-day oceans [*Pennington et al.*, 2006]. Relatively high year-round primary productivity levels are responsible for relatively high sedimentation rates on the order of 2.5 to 3.0 cm kyr^{-1} for the past 5 Myr [*Mayer et al.*, 1985; *Mix et al.*, 1995], allowing the generation of highly temporally resolved proxy records in this region. However, given the supply of upwelled nutrient-rich waters, modern biological production in the EEP is not as high as we might expect because of iron limitation [*Coale et al.*, 1996], characterizing the EEP Ocean as a high-nutrient, low-chlorophyll (HNLC) region.

During the late Pliocene, large ice sheets were established on North America and Eurasia [e.g., *Shackleton et al.*, 1984; *Bailey et al.*, 2013] probably in response to a slow decline in carbon dioxide levels and therefore global temperature [*DeConto et al.*, 2008; *Lunt et al.*, 2008]. This so-called "intensification of Northern Hemisphere glaciation" (iNHG) resulted in large productivity changes in the oceans on both secular and glacial-interglacial (G-IG) timescales. At the global scale proxy records for export productivity demonstrate high-latitude productivity shifts [e.g., *Hillenbrand and Fütterer*, 2001; *Bolton et al.*, 2011] that are broadly coincident with but opposite in sign to (sub)tropical productivity patterns in upwelling regions [e.g., *Lawrence et al.*, 2006, 2013; *Bolton et al.*, 2011]. The

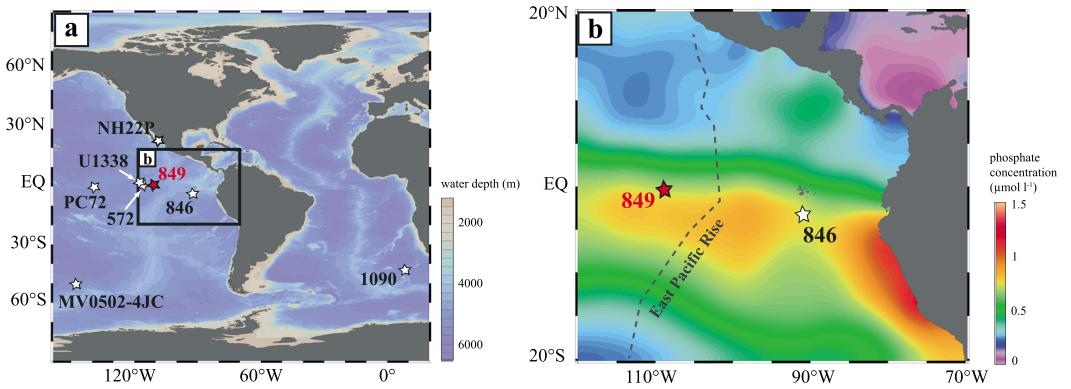

Figure 1. (a) Bathymetric map showing the location of ODP Site 849 (red; this study) and other sites mentioned in the text (white). Water depth (m) is shown after World Ocean Atlas. (b) Location map of ODP Sites 849 (red; this study) and 846 (white). Modern annual sea surface phosphate concentrations (μmol L^{-1}) are shown after World Ocean Atlas [*Garcia et al.*, 2014].

mechanisms driving these low-latitude productivity fluctuations are a subject of ongoing debate with hypotheses including changes in trade wind strength/upwelling intensity ("upwelling hypothesis") [see *Cleaveland and Herbert*, 2007; *Etourneau et al.*, 2010] and/or changes in the nutrient content of the upwelled water masses ("nutrient delivery hypothesis") [see *Lawrence et al.*, 2006, 2013; *Bolton et al.*, 2011; *Lyle and Baldauf*, 2015].

Here we present new proxy records of suborbital resolution from Ocean Drilling Program (ODP) Site 849 to shed new light on the dynamics and the origin of G-IG productivity changes in the EEP. We analyzed the time interval from 2.65 to 2.4 Ma (marine isotope stage (MIS) G1 to 94, latest Pliocene/early Pleistocene following *Gibbard et al.* [2010]), including the first three consecutive large-amplitude (~1‰ in benthic δ^{18}O [*Lisiecki and Raymo*, 2005]) G-IG cycles (MIS 100 to 96) representing the culmination of late Pliocene iNHG. Marine isotope stage 100 has particular significance because it was the first glacial during which (i) the Laurentide Ice Sheet (LIS) advanced into the midlatitudes [*Bailey et al.*, 2010; *Balco and Rovey*, 2010; *Lang et al.*, 2014] and (ii) ice rafting first became widespread across the North Atlantic Ocean [e.g., *Shackleton et al.*, 1984; *Kleiven et al.*, 2002; *Naafs et al.*, 2013] with ice-rafted debris flux and provenance in the subpolar North Atlantic comparable to that of the Last Glacial Maximum (LGM) [*Bailey et al.*, 2013]. Advance of the LIS into the midlatitudes has important implications for atmospheric circulation and hydroclimate regionally [*Bailey et al.*, 2010; *Hennissen et al.*, 2014; *Lang et al.*, 2014; *Oster et al.*, 2015] and may also have influenced the behavior and dynamics of upwelling in the EEP. Here we use suborbitally resolved sand accumulation rates in combination with lower resolution planktic foraminiferal fragmentation and planktic foraminiferal and radiolarian accumulation rates from Site 849 as a productivity proxy [e.g., *Diester-Haass et al.*, 2002] to compare with an alkenone-based paleoproductivity record from ODP Site 846 [*Lawrence et al.*, 2006] (Figures 1a and 1b). We also generated suborbitally resolved δ^{13}C records in three foraminiferal species (shallow-dwelling planktic, thermocline-dwelling planktic, and benthic) to investigate the potential influence of different water masses at the study site [e.g., *Mackensen et al.*, 2001; *Curry and Oppo*, 2005] and to evaluate δ^{13}C gradients between the sea surface and thermocline, shedding new light on changes in thermocline depth and thus upwelling intensity [e.g., *Pierre et al.*, 2001].

2. Modes and Drivers of Past Variability in Eastern Equatorial Pacific Productivity During the Plio-Pleistocene

Biological production underwent a progressive decrease in the high-latitude oceans during iNHG while increasing in low- to middle-latitude settings [e.g., *Sarnthein and Fenner*, 1988; *Bolton et al.*, 2011; *Etourneau et al.*, 2012; *Lawrence et al.*, 2013]. Different driving mechanisms have been proposed to explain the secular shift toward a more productive regime in low latitudes during Pliocene iNHG. The (sub)tropical productivity increase is suggested to result (i) from a shoaling of the tropical thermocline/upwelling intensification, predominantly depending on the trade wind strength and thus the equator-to-pole temperature gradient [*Pisias and Mix*, 1997, and references therein; *Cleaveland and Herbert*, 2007; *Etourneau et al.*, 2010], and/or (ii) from a reorganization of the nutrient content in high southern latitude surface waters [*Lawrence et al.*, 2006, 2013; *Bolton et al.*, 2011; *Lyle and Baldauf*, 2015] that feed low-latitude upwelling regions [*Tsuchiya et al.*, 1989; *Toggweiler et al.*, 1991]. Over the early and middle Miocene, a major source for the waters upwelled in the EEP was the deep water

formed in the higher-latitude Southern Ocean, as evidenced by small benthic carbon isotope gradients [*Poore et al*., 2006; *Cramer et al*., 2009] and neodymium isotope records [*Holbourn et al*., 2013] across the Pacific Ocean basin. Over the course of the Neogene, the export of Southern Ocean deep water to the lower latitude Pacific generally increased [*van de Flierdt et al*., 2004], ultimately culminating in the present-day situation where upwelled waters in the EEP are primarily sourced from the Southern Ocean with an insignificant contribution from the North Pacific [*Tsuchiya et al*., 1989; *Toggweiler et al*., 1991]. Hence, long-term shifts in the rate of primary productivity in the EEP are controlled not only by the strength of upwelling but also by the chemical composition of the source waters. Long-term changes in Southern Ocean source water properties such as increasing nutrient contents may have been regulated by a secular increase in sea ice coverage [*Hillenbrand and Cortese*, 2006], stronger water column stratification [*Haug et al*., 1999], and/or a long-term equatorward shift in the position of the Southern Ocean westerly winds [*Lawrence et al*., 2013], inducing a high-latitude productivity crash in step with a subpolar and middle- to low-latitude productivity increase during iNHG at ~2.5 Ma [*Lawrence et al*., 2013, and references therein].

In addition to the secular productivity increase in (sub)tropical upwelling regimes during iNHG, G-IG productivity fluctuations in low latitudes became more pronounced, strongly paced by Earth's obliquity (41 kyr) [*Lawrence et al*., 2006]. It has been demonstrated that low-latitude productivity was elevated during glacials compared to interglacials [*Lawrence et al*., 2006; *Bolton et al*., 2010a] and that the amplitude of these G-IG productivity fluctuations increased across iNHG [*Lawrence et al*., 2006]. To explain the variability in biological production on G-IG timescales, two competing hypotheses have been proposed, invoking either changes in the upwelling intensity [*Cleaveland and Herbert*, 2007; *Etourneau et al*., 2010] or changes in the nutrient availability within the upwelled water masses in the low latitudes [*Lawrence et al*., 2006; *Etourneau et al*., 2013] or a combination of both factors [*Filippelli et al*., 2007]. Traditionally, it has been argued that observed G-IG changes in EEP primary productivity were linked to variations in upwelling rates in response to modified trade wind strengths [e.g., *Bjerknes*, 1969; *Etourneau et al*., 2010], a process that has been also proposed for late Pleistocene glacials [e.g., *Pisias and Mix*, 1997, and references therein]. In this interpretation, an increased equator-to-pole temperature gradient during glacials acts to trigger a strengthening of the trade winds and therefore upwelling of cold nutrient-rich waters leading to a simultaneous increase in biological production (the upwelling hypothesis). However, more recent studies from EEP upwelling zones suggest that primary productivity and temperature were decoupled from one another during the past 5 Myr, a scenario that is incompatible with upwelling strength being the only driver of productivity changes [*Loubere*, 2000; *Dekens et al*., 2007]. These observations have led to the suggestion that the productivity increase during Plio-Pleistocene glacials recorded in the EEP may have primarily resulted from an enhanced nutrient content in upwelled waters sourced from the high southern latitudes [*Lawrence et al*., 2006; *Etourneau et al*., 2013]. In this interpretation, the strength of the upwelling system plays a subordinate role in modulating EEP G-IG productivity changes. Instead, climate conditions in the higher-latitude Southern Ocean and primary productivity and thus nutrient utilization in that region control the nutrient content of upwelled EEP waters on G-IG timescales (the nutrient delivery hypothesis).

Regardless of which of these two hypotheses holds true, G-IG primary productivity changes may also be influenced by aeolian dust input [e.g., *McGee et al*., 2007; *Winckler et al*., 2008; *Lang et al*., 2014], especially in HNLC ecosystems such as the EEP where nutrient concentrations are high, but biological production is limited by iron availability [*Coale et al*., 1996]. Because dust serves as a natural source of iron and other micronutrients [*Winckler et al*., 2008], higher glacial than interglacial dust fluxes sourced in northern South America [*Nakai et al*., 1993; *Stancin et al*., 2006] may have resulted in an additional increase (decrease) in biological production during glacials (interglacials). Enhanced glacial dust fluxes are suggested to have driven increased productivity for at least the past five G-IG cycles within the EEP [*McGee et al*., 2007; *Winckler et al*., 2008]. On the other hand, a study of central equatorial Pacific spanning the Miocene to Holocene demonstrated no systematic relationship between iron input or pathway and total biological export production for Pleistocene G-IG cycles [*Ziegler et al*., 2008].

In this study we test the competing hypotheses for G-IG productivity change in the EEP during the latest Pliocene to earliest Pleistocene.

3. Site Description

All Plio-Pleistocene EEP productivity records on G-IG timescales used in support of either the upwelling hypothesis or the nutrient delivery hypothesis come from sites located east of the East Pacific Rise (EPR;

Figure 1b). To quantify changes in primary productivity within the open ocean equatorial Pacific, we investigated sediments from Site 849 (0°11′N, 110°31′W; Figures 1a and 1b), which is located ~860 km west of the EPR; thus, it records a more global ocean signal [*Mix et al*., 1995]. Site 849 was drilled during ODP Leg 138 in 1991 [*Mayer et al*., 1992]. A nearly complete sequence of late Miocene to Holocene sediments was recovered [*Mayer et al*., 1992]. Site 849 is situated at a present-day water depth of 3851 m [*Mix et al*., 1995], close to the modern lysocline in the equatorial Pacific (3.2–3.4 km water depth [*Adelseck and Anderson*, 1978; *Berger et al*., 1982]) and well above the carbonate compensation depth (estimated deeper than 4.5 km water depth in the equatorial Pacific during the Plio-Pleistocene transition [*Pälike et al*., 2012]). Site 849 is positioned in the present-day equatorial divergence zone within the so-called "cold tongue" [*Wyrtki*, 1981] where convergent trade winds from the Northern and Southern Hemispheres induce the year-around upwelling of cold, nutrient-rich waters from below the thermocline to the surface.

Changes in the paleoposition of Site 849 were negligible over the past 4 Myr [*Pisias et al*., 1995], but our geographical (EEP) and stratigraphic (Plio-Pleistocene boundary) focus means that the closure of the Central American Seaway (CAS) has the potential to influence paleoceanographic records from Sites 849 and especially 846 (Figure 1). Global climate-ocean ecosystem model experiments suggest that the first-order effect of CAS closure is likely to have promoted increased upwelling rates and surface water nutrient concentrations in the EEP [*Schneider and Schmittner*, 2006]. The timing of this closure has received considerable recent attention, and it is important to understand what is meant by the terms open versus closed. The CAS may maintain a shallow ($<$50 m) connection between the EEP and the Caribbean Sea but be effectively closed with respect to its influence on ocean circulation, while the migration of mammals between North and South America requires a continuous land bridge [*Groeneveld et al*., 2014]. Some studies place CAS closure (i.e., cutoff of deep water connection between the EEP and the Caribbean Sea) in the mid-Miocene [e.g., *Sepulchre et al*., 2014], whereas other investigations point to a surface water exchange between the EEP and the Caribbean Sea until the late Pliocene [*Steph et al*., 2010] with temporary glacioeustatic sea level-led gateway closures with a significant impact on ocean circulation during prominent iNHG glacials [*Groeneveld et al*., 2014].

4. Methods

4.1. Sampling

To study our target interval centered on MIS 100 to 96, we sampled cores 849C-7H-1-96 cm to 849C-7H-1-146 cm, 849D-6H-5-125 cm to 849D-6H-7-16 cm, and 849D-7H-1-0 cm to 849D-7H-3-55 cm (74.16 to 67.78 m composite depth (mcd)). To generate a record at suborbital resolution (mean ~780 years), 20 cm^3 samples were taken at 2 cm intervals. The sampled core material consists of biogenic sediment without clay components—a white to light grey nannofossil ooze [*Mayer et al*., 1992]. Samples were dried, weighed, and washed over a 63 μm sieve. The coarse residue (sand fraction) primarily consists of $CaCO_3$-producing organisms, namely, planktic and benthic foraminifera together with siliceous radiolarians (see Figure S1 in the supporting information). The fine fraction, in turn, is predominantly composed of calcareous nannoplankton (coccoliths) together with rare siliceous diatoms [*Mayer et al*., 1992; *Flores et al*., 1995].

4.2. Stable-Isotope Analysis

A total of 229 samples from ODP Site 849 between 74.16 and 67.78 mcd were analyzed for foraminiferal stable oxygen and carbon isotope compositions ($\delta^{18}O$ and $\delta^{13}C$).

To develop the benthic $\delta^{18}O$ and $\delta^{13}C$ records, an average of six specimens of the benthic foraminifera *Cibicidoides wuellerstorfi* were picked from the $>$150 μm dried sediment fraction of all samples. The resulting data set was supplemented by the data set of *Mix et al*. [1995] (35 samples also based on *C. wuellerstorfi*), yielding a total of 264 stable-isotope data points for our $\delta^{18}O$ and $\delta^{13}C$ stratigraphy.

Specimens of the planktic foraminifera *Globigerinoides ruber* (white) were used to characterize the sea surface $\delta^{13}C$ variability across the study interval. We used the morphotype *G. ruber* sensu stricto (s.s.), which thrives in shallower waters of the upper mixed layer than *G. ruber* sensu lato (s.l.) and thus yields lower $\delta^{18}O$ and higher $\delta^{13}C$ values [e.g., *Wang*, 2000; *Steinke et al*., 2005]. On average, 11 specimens of *G. ruber* s.s were picked per sample. A narrow size range of 250–315 μm was chosen to avoid ontogenetic effects [*Elderfield et al*., 2002; *Friedrich et al*., 2012].

To monitor changes in the thermocline, we followed the approach of *Ravelo and Fairbanks* [1992] and *Kemle von Mücke and Oberhänsli* [1999] and generated a δ^{13}C record of the planktic foraminifera *Globorotalia crassaformis*. To avoid ontogenetic effects, *G. crassaformis* was picked from the 315–400 μm dried sediment fraction [*Elderfield et al*., 2002]. An average of 19 specimens was picked per sample. Many planktic foraminifera, such as *G. crassaformis*, have a dextral and a sinistral coiling form. We preferentially selected the most abundant coiling direction (sinistral). However, the sinistral coiling forms did not occur continuously over the sampling interval. Thus, we also used the dextral coiling tests for some intervals. Comparison between δ^{13}C measurements of sinistral and dextral coiling forms within the same samples indicates that there is no defined offset in δ^{13}C between specimens with different coiling directions (see Figure S2 in the supporting information). Thus, whenever required, we spliced together records of sinistral and dextral coiling forms of *G. crassaformis* without applying an intertaxon adjustment factor.

Stable isotopes were measured at the Institute of Geosciences, Goethe University Frankfurt (Germany), using a ThermoFinnigan MAT253 gas source mass spectrometer equipped with a Gas Bench II. The results are reported relative to Vienna Peedee belemnite (VPDB) through the analysis of an in-house standard calibrated to NBS-18 and NBS-19. Analytical precision was better than 0.08‰ and 0.06‰ (at 1σ level) for oxygen and carbon isotopes, respectively. Following *Shackleton and Hall* [1984], δ^{18}O values of *C. wuellerstorfi* reported herein were adjusted for species-specific offset from equilibrium by the addition of +0.64‰. *Cibicidoides wuellerstorfi* precipitates its shell close to δ^{13}C equilibrium; thus, no adjustment factor is required [e.g., *Zahn et al*., 1986; *Mackensen et al*., 1993]. δ^{13}C values of *G. ruber* were adjusted by the addition of +0.94‰ according to the δ^{13}C normalization of *Spero et al*. [2003]. The lack of laboratory investigations into δ^{13}C fractionation in *G. crassaformis* dictates that we simply report the δ^{13}C values measured on this species (no adjustment factor).

4.3. Preservation of Foraminiferal Tests

To assess the preservation of planktic foraminiferal tests used for stable-isotope analysis at Site 849, selected specimens representing both glacial and interglacial intervals were examined using a LEO 440 scanning electron microscope (SEM) at the Institute of Earth Sciences, Heidelberg University. Further, we determined a planktic foraminiferal fragmentation index (FFI) at G-IG resolution following *Le and Shackleton* [1992] and *Le et al*. [1995]:

$$\mathrm{FFI}[\%] = (\text{number of fragments}/8)\times(\text{number of fragments}/8 + \text{complete tests})^{-1}\times 100\%$$

The number of fragments (part of a test which is less than two thirds of an original test [*Berger et al*., 1982]) and of complete planktic foraminiferal tests was counted on at least 300 specimens (using a microsplitter) from aliquots of the >150 μm size fraction. The number of fragments was divided by 8 because a foraminiferal test on average splits into eight fragments (*Le and Shackleton* [1992] and *Saraswat* [2015] for a review).

4.4. Sand, Foraminiferal, and Radiolarian Accumulation Rates

To identify changes in sea surface productivity in these biogenic sediments, accumulation rates of the sand fraction (SAR; suborbital resolution), of planktic foraminifera (PFAR; G-IG resolution), and of radiolarians (RAR; G-IG resolution) were calculated according to *Herguera and Berger* [1991]:

$$\mathrm{SAR}\ \left[\mathrm{g\ cm^{-2}kyr^{-1}}\right] = \mathrm{DBD}\times\mathrm{LSR}\times\mathrm{SF}$$

$$\mathrm{PFAR}\left[\text{number of specimens cm}^{-2}\mathrm{kyr}^{-1}\right] = \mathrm{DBD}\times\mathrm{LSR}\times\mathrm{PF}$$

$$\mathrm{RAR}\ \left[\text{number of specimens cm}^{-2}\mathrm{kyr}^{-1}\right] = \mathrm{DBD}\times\mathrm{LSR}\times R$$

where DBD is the dry bulk density (g cm^{-3}), LSR is the linear sedimentation rate (cm kyr^{-1}), SF is the portion of the >63 μm sand fraction per gram dry sediment, PF is the number of planktic foraminifera per gram dry sediment (>63 μm), and R is the number of radiolarians per gram dry sediment (>63 μm). The number of planktic foraminifera and radiolarians was counted on at least 300 specimens (using a microsplitter) from aliquots of the >63 μm fraction. Because the resolution of available DBD data for the herein investigated time interval at Site 849 is insufficient, DBD was calculated from high-resolution GRAPE density (g cm^{-3}) shipboard measurements (IODP JANUS database [*Mayer et al*., 1992]) using an equation developed for lithologic homogeneous samples of Hole 849B [*Hovan*, 2013] as a reference ($R^2 = 0.93$, $p < 0.01$, number of samples = 158; see Figure S3 in the supporting information):

$$\mathrm{DBD}\ \left[\mathrm{g\ cm^{-3}}\right] = 1.58\times\mathrm{GRAPE}–1.61$$

4.5. Cross-Spectral Analyses

To identify coherencies and to quantify phase lags between records, Blackman-Tukey cross-spectral analyses with 30% overlap were conducted using the AnalySeries software package version 2.0.8 [*Paillard et al*., 1996]. Data for cross-spectral analyses were linearly interpolated, detrended, and prewhitened.

5. Results and Discussion

5.1. Chronology

Our age model for Site 849 (Figure 2 and Table S1 in the supporting information) was constructed by visual correlation of the benthic oxygen isotope record (including benthic δ^{18}O data of *Mix et al*. [1995]) to the LR04 stack [*Lisiecki and Raymo*, 2005] using the AnalySeries software package version 2.0.8 [*Paillard et al*., 1996]. To minimize errors during tuning, only one tie point at the midpoint of each G-IG δ^{18}O transition was used [e.g., *Bolton et al*., 2010b].

Our high-resolution δ^{18}O record of *C. wuellerstorfi* shows a clear G-IG cyclicity, with lower values during interglacial stages (mean: 3.52‰; minimum value: 3.02‰) and highest values during glacial stages (mean: 3.89‰; maximum value: 4.31‰; Figures 2a and 2b). The spike in benthic δ^{18}O during MIS 102, which represents the lowest values of the entire record, consists of two independently generated data points (this study and *Mix et al*. [1995]). Core images taken during core sampling show no sign of local reworking for this core section. Therefore, it appears reasonable to assume that this spike is real, albeit peculiar.

The new chronology for Site 849 results in a mean temporal sample resolution of 780 years and an average linear sedimentation rate of 2.6 cm kyr^{-1} (Figure 2c) for the time interval between 2.65 and 2.4 Ma (MIS G1 to 94). These sedimentation rates are in close agreement with those of other records published for the late Pliocene/early Pleistocene from the EEP region (e.g., Deep Sea Drilling Project Site 572: 2.1 cm kyr^{-1} [*Mayer et al*., 1985] (Figure 1a) and ODP Site 849: 2.5–3.0 cm kyr^{-1} [*Mix et al*., 1995]).

We also decided to retune the benthic δ^{18}O record from Site 846 [*Shackleton et al*., 1995] to the LR04 stack [*Lisiecki and Raymo*, 2005] over the time interval 2.65 to 2.4 Ma (Figures 3a and 3b and Table S2 in the supporting information) although these benthic δ^{18}O data are part of the LR04 stack. Reasons for this are threefold: (1) The Site 846 δ^{18}O record is not an initial alignment target (using original terminology of *Lisiecki and Raymo* [2005, p. 5]) for the LR04 stack for the time interval investigated in this study, i.e., 23 more δ^{18}O records besides the δ^{18}O record from Site 846 feed the LR04 stack between 2.65 and 2.4 Ma [*Lisiecki and Raymo*, 2005]. (2) Comparison of the δ^{18}O record from Site 846 [*Shackleton et al*., 1995] with LR04-tuned benthic δ^{18}O from Site 849 demonstrates significant discrepancies (Figure 3c). This is most likely a consequence of the different tuning techniques. (3) Therefore, exactly the same tuning procedures have been applied (i.e., using only one tie point at the midpoint of each G-IG δ^{18}O transition) to allow for the best possible comparison between sites.

5.2. Preservation of Planktic Foraminiferal Tests

While low-resolution shipboard investigations on core catchers report poor preservation of planktic foraminiferal tests at Site 849 [*Mayer et al*., 1992], none of these observations correspond to samples from our study interval. Scanning electron microscope images of both glacial and interglacial samples from our sample set indicate that the preservation of planktic foraminifers is consistently good enough to acquire high-quality stable-isotope data [see *Sexton et al*., 2006] throughout the target interval (Figure 4). This interpretation is confirmed by relatively low mean FFIs at Site 849 (~5%, Figure 5b) compared to previous published FFIs from Site 846 for the last 0.8 Myr (~9% [*Le et al*., 1995]) and from Site 849 for the last G-IG cycle (~6 to 18% [*Marchitto et al*., 2005]), indicating that the effect of dissolution on planktic foraminiferal tests was minor throughout our study interval. Furthermore, in contrast to the late (early) Pleistocene Pacific Ocean carbonate dissolution pattern, in which maximum fragmentation is usually seen during interglacials (glacials) [e.g., *Le and Shackleton*, 1992; *Le et al*., 1995; *Marchitto et al*., 2005; *Lalicata and Lea*, 2011; *Sexton and Barker*, 2012], FFIs at Site 849 show no G-IG pattern over the interval of study. This is evidenced by a lack of a statistically significant correlation between FFI and benthic δ^{18}O at Site 849 throughout the interval of study ($R^2 = 0.004$, $p = 0.74$; see Figure S4a in the supporting information).

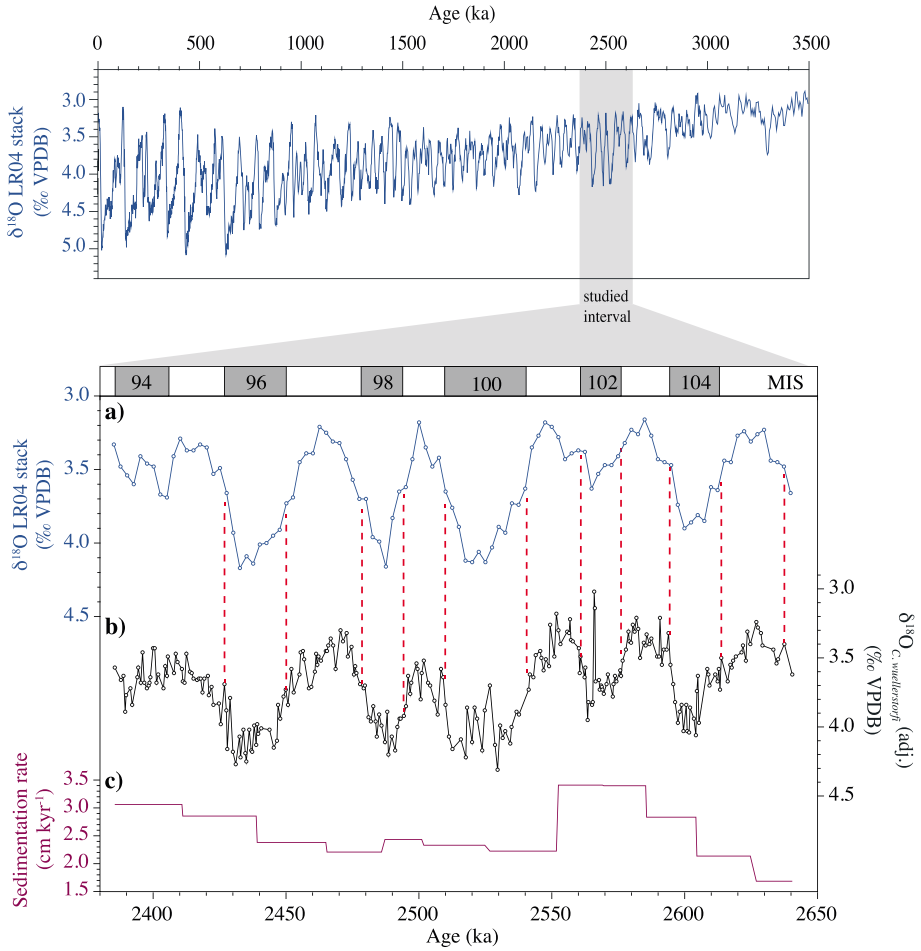

Figure 2. Global benthic foraminiferal δ^{18}O record [*Lisiecki and Raymo*, 2005] for the last 3.5 Myr (LR04 stack) (top). Age model from ODP Site 849 for MIS G1 to 94 (2640 to 2385 ka), tuned to the LR04 stack [*Lisiecki and Raymo*, 2005] (bottom). (a) LR04 stack for MIS G1 to 96 [*Lisiecki and Raymo*, 2005]. (b) Benthic foraminiferal (*C. wuellerstorfi*) δ^{18}O record from Site 849; this record contains a combination of our own measurements and data from *Mix et al.* [1995]. (c) Average linear sedimentation rates (cm kyr^{-1}). Red dashed lines in Figures 2a and 2b show the tie points for tuning. Tuning points are provided in Table S1.

5.3. Glacial-Interglacial Variations in the Sand Accumulation Rate as a Tracer for Paleoproductivity

The SAR record at Site 849 shows a clear G-IG cyclicity from MIS 100 onward, with lowest values toward the end of each interglacial-to-glacial transition (minimum value: 0.04 g cm^{-2} kyr^{-1}) and progressively increasing values starting at peak glacials and culminating at glacial terminations (maximum value: 0.22 g cm^{-2} kyr^{-1}; Figure 5c). Such G-IG variations also seem to appear prior to MIS 100, but that signal is much less distinct. There are at least three processes to consider when interpreting this record. First, SARs in deep-sea sites are often interpreted as an indicator of carbonate dissolution [e.g., *Johnson et al.*, 1977; *Wu et al.*, 1990; *Bassinot et al.*, 1994]. A second possibility is that changes in the sand fraction are controlled by changes in export productivity [*Diester-Haass et al.*, 2002], and a third possibility is that SARs are controlled by the strength of bottom water currents leading to winnowing [*Berstad et al.*, 2003]. Although we cannot completely rule out sediment redistribution as a controlling mechanism for SARs at Site 849 [e.g., *Pichat et al.*, 2004], present-day bottom water current speeds in this region are generally less than ~10 cm s^{-1} [*Johnson*, 1972], i.e., too sluggish to redistribute coarser particles [*Beaulieu*, 2002]. Therefore, we suggest that in a deep open ocean setting such as the deep equatorial Pacific with a relatively flat topography, sand redistribution by the relatively weak deep-sea bottom water currents is unlikely [*Paytan et al.*, 2004]. Based on the lack of statistically significant correlation between SAR and FFI ($R^2 = 0.03$, $p = 0.35$; see Figure S4b in the supporting information), we also exclude a major influence of carbonate dissolution on SAR (see also section 5.2).

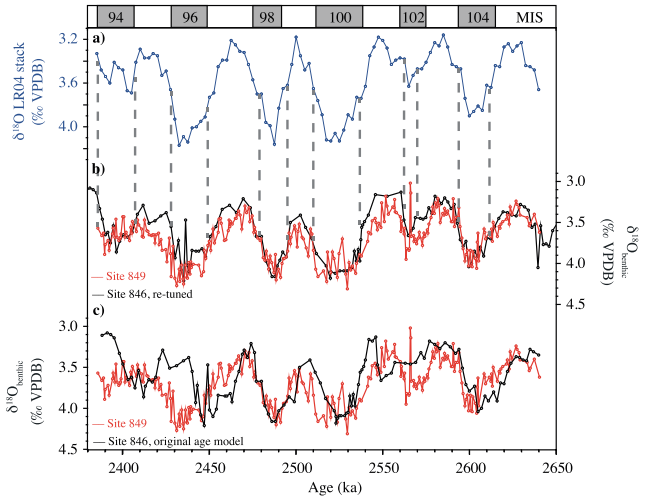

Figure 3. Age model from ODP Site 846 for MIS G1 to 94 (2640 to 2385 ka). (a) LR04 stack for MIS G1 to 96 [*Lisiecki and Raymo*, 2005]. (b) Retuned benthic foraminiferal $\delta^{18}O$ record from Site 846 (black) compared to benthic foraminiferal $\delta^{18}O$ from Site 849 (red). (c) Benthic foraminiferal $\delta^{18}O$ record from Site 846 (original age model (black) [*Shackleton et al.*, 1995]) and Site 849 (red). Grey dashed lines in Figures 3a and 3b show the tie points for tuning. Tuning points are provided in Table S2.

The vast majority of the >63 μm size fraction consists of planktic foraminifera and radiolarians (together with rare benthic foraminifera; see section 4.1 and Figure S1). Thus, variations in the sand fraction predominantly reflect changes in zooplankton accumulation. Having ruled out a major role for carbonate dissolution (see also section 5.2), burial rates of zooplankton are controlled by rain rates from the surface ocean, which in turn are strongly coupled to surface ocean primary production [e.g., *Reynolds and Thunell*, 1985; *Eguchi et al.*, 1999]. Therefore, changes in our SARs can be considered a measure of surface water productivity. Based on this notion, our SAR record together with planktic foraminiferal and radiolarian accumulation rates (Figures 5c–5e) suggest that biological production at Site 849 fluctuated strongly on G-IG timescales. As depicted in Figures 5c–5e, productivity at Site 849 progressively increased from peak glacial to glacial termination (high SARs, PFARs, and RARs), and SAR (i.e., export productivity) lags benthic $\delta^{18}O$ by ~9.5 kyr (Figure 6 and section 6.2). Increased export productivity is expected to result in elevated sedimentation rates. At Site 849, however, a lack of statistically significant correlation between SAR and LSR ($R^2 = 0.07$, $p = 0.15$; see Figure S5a in the supporting information) suggests that there must be a counterbalancing factor to smooth out sedimentation rates. We suggest that decreases (increases) in the fraction of poorly packed spinose radiolarians during glacials (interglacials) relative to the number of planktic foraminifera act to cancel out productivity-related changes in sedimentation rates (Figures 5d and S5b in the supporting information).

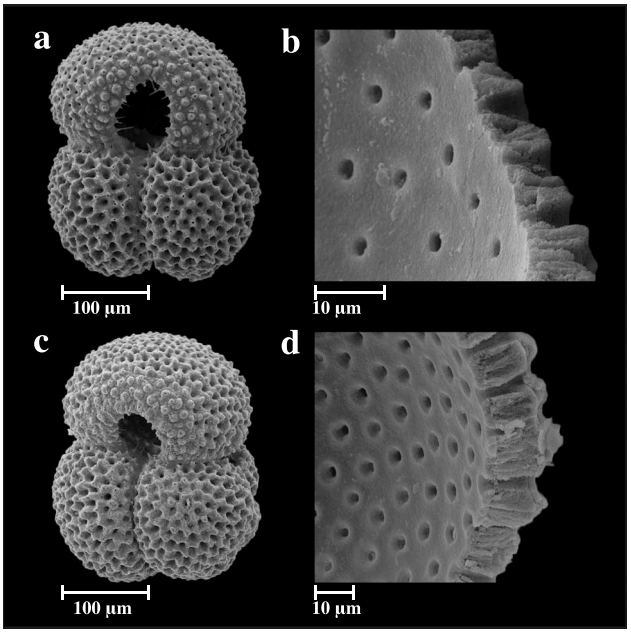

Figure 4. Scanning electron micrographs of *Globigerinoides ruber* (s.s.) from EEP Site 849. Both interglacial (a, b) (sample 849D-6H-6-6 cm to 849D-6H-6-8 cm) and glacial (c, d) (sample 849C-7H-1-146 cm to 849C-7H-1-148 cm) foraminiferal tests are well preserved, allowing for the acquisition of reliable stable-isotope data. Note the preservation of delicate spines in the aperture region.

Contrary to our findings from Site 849, observations from ODP Site 846 (Figure 5f) based on C_{37} alkenone accumulation rates [*Lawrence et al.*, 2006], and calcareous nannofossil assemblages and siliceous fragment fluxes [*Lawrence et al.*, 2006; *Bolton et al.*, 2010a], demonstrate that primary productivity was highest during full glacials MIS 104, 100, 98, and 96, nearly in phase with benthic $\delta^{18}O$ (lead of ~2 to 3 kyr [*Lawrence et al.*, 2006]; see also Figure S6 in the supporting information). There are at least two processes to consider when interpreting these findings.

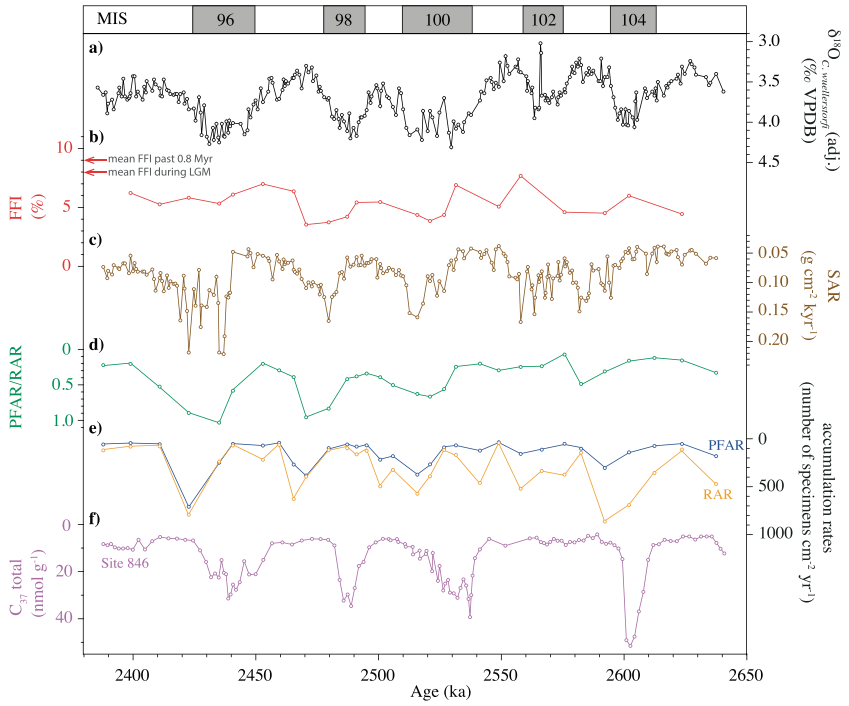

Figure 5. Dissolution and productivity proxy records from the EEP upwelling system. (a) $\delta^{18}O$ in benthic foraminifera (*C. wuellerstorfi*) from Site 849 (this study). (b) Percentage planktic foraminiferal fragmentation from Site 849 (this study). Red arrows depict mean FFIs for the past 0.8 Myr at Site 846 (~9% [*Le et al.*, 1995]) and for the LGM at Site 849 (~8% [*Marchitto et al.*, 2005]). Holocene FFIs reach ~16% at Site 849 [*Marchitto et al.*, 2005] and ~30% [*Le et al.*, 1995] at Site 846. (c) Sand accumulation rates (>63 μm) from Site 849 (this study). (d) Ratio between planktic foraminiferal and radiolarian accumulation rates at Site 849 (this study). (e) Planktic foraminiferal accumulation rates (blue) and radiolarian accumulation rates (orange) at Site 849 (this study). (f) C_{37} alkenone abundances from Site 846 [*Lawrence et al.*, 2006] retuned to the LR04 stack.

First, productivity records from Site 849 and 846 are based on different proxies, namely, zooplankton (Site 849) and haptophyte algae (Site 846). Second, the observed lag of ~11 kyr in peak productivity between Site 849 (SAR, termination) and Site 846 (C_{37} alkenone accumulation rates, nearly peak glacial) represents a real time lag that is too large to result from age model discrepancies (Figures 3, 6, and S6), suggesting that biological production at Sites 846 and 849 was regulated by different mechanisms at least during these late Pliocene/early Pleistocene glacials. We note that secular timescale changes in export productivity over the Plio-Pleistocene also appear to be decoupled between Sites 846 and 849 [*Ma et al.*, 2015], suggesting that different mechanisms or nutrient sources drive productivity in these two distinct regions of the highly heterogeneous EEP [*Pennington et al.*, 2006].

It has been suggested that the Panamanian Gateway was closed during MIS 100 to 98, opened during MIS 97, and closed again toward the end of MIS 96 [*Groeneveld et al.*, 2014]. Assuming that CAS closure helps to promote upwelling in the EEP [*Schneider and Schmittner*, 2006], we might expect these closures to result in increased export production during MIS 100, 99, and 98, low productivity rates during MIS 97, and again enhanced productivity toward the end of MIS 96. However, this is not consistent with our SAR record at least for MIS 100 to 98, which documents significant G-IG changes in export production at Site 849 between MIS 100, 99, and 98 (Figures 5c and S7 in the supporting information). Thus, we suggest that the influence of temporary full CAS closure on upwelling intensification at Site 849 plays only a minor role in regulating G-IG upwelling changes across the studied succession. Furthermore, we find no evidence to suggest that dust input played a major role in controlling the observed changes in export production at Site 849. The reasons for this interpretation are twofold: (1) in our records maximum productivity occurs during glacial terminations at least during MIS 100, 98, and 96 (Figure 5 c), while, based on late Pleistocene records, we might expect dust input at Site 849 to have peaked during full glacial conditions [*McGee et al.*, 2007; *Winckler et al.*, 2008], and (2) low-resolution data on aeolian dust flux from Leg 138 yield no evidence for G-IG changes in dust input to the EEP across the studied time interval [*Hovan*, 1995]. This interpretation is consistent with a study of export production from the central equatorial Pacific covering iNHG, indicating that iron supply is not responsible for changes in export production [*Ziegler et al.*, 2008].

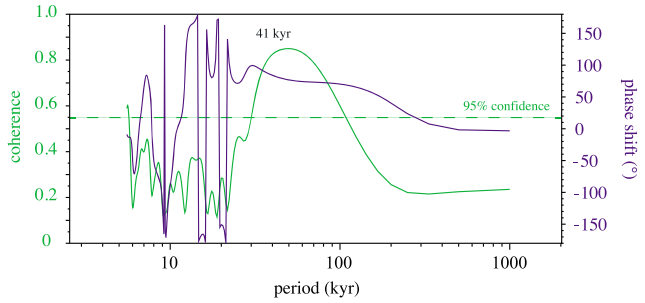

Figure 6. Blackman-Tukey cross-spectral analysis for the identification of phase shifts at Site 849 for the time interval from ~2.65 to 2.4 Ma at the 95% confidence level. Coherence (green) and phase (purple) relationship between global ice volume ($\delta^{18}O_b$) and productivity (SAR) from Site 849 are plotted on log scales. Positive values in this phase plot indicate that productivity lags global ice volume, i.e., by 82.2° (equal to –9.5 kyr) for the 41 kyr period.

To decipher the importance of wind-driven upwelling versus mode water nutrient supply on observed G-IG changes in primary productivity at Site 849, we use the carbon isotope signature of benthic, thermocline-, and sea surface-dwelling foraminiferal species.

5.4. $\delta^{13}C$ Values at Site 849 Trace Glacial-Interglacial Changes in Delivery of Macronutrients to the Equatorial Pacific From the Southern Ocean

The $\delta^{13}C$ signature of foraminiferal tests is routinely used as a proxy for surface water primary productivity [e.g., *Zahn et al*., 1986; *Sarnthein et al*., 1988; *Mackensen and Bickert*, 1999]. An increase in primary productivity during times with a strong and efficient biological pump increases $\delta^{13}C$ values in the surface water (traceable in surface-dwelling planktic foraminifera, $\delta^{13}C_s$) and progressively decreases $\delta^{13}C$ values with increasing water depth (recorded in thermocline-dwelling planktic foraminifera, $\delta^{13}C_t$, and benthic foraminifera, $\delta^{13}C_b$). In our data set, all three $\delta^{13}C$ records show a clear G-IG cyclicity with higher $\delta^{13}C$ values during interglacials and lower $\delta^{13}C$ values during glacials (Figures 7a–7d). This trend is weak, however, during MIS 102 suggesting that associated environmental change during this modest glacial was too subtle to induce larger-scale changes in the mechanisms that controlled benthic and planktic foraminiferal $\delta^{13}C$. The parallel trends and relatively constant gradients in our $\delta^{13}C_b$ (*C. wuellerstorfi*) and $\delta\ ^{13}C_{s,t}$ (*G. ruber* and *G. crassaformis*) records (Figures 7b–7d and S8 in the supporting information) suggest that the foraminiferal $\delta^{13}C$ at Site 849 does not simply trace in situ changes in the strength of the biological pump during the interval of study, and an alternative explanation for the observed pattern is required.

We must also consider the possibility that our $\delta^{13}C$ records reflect changes in the isotopic signature of source waters (Southern Ocean Water (SOW) and Antarctic Bottom Water (AABW)) that feed the equatorial Pacific upwelling system. For our interval of study, the best available $\delta^{13}C_b$ records for approximating isotopic change in Southern Ocean waters end-member values [*Billups et al*., 2002; *Pusz et al*., 2011] are those from South Pacific Site MV0502-4JC (50°20'S, 148°08'W, 4286 m water depth [*Waddell et al*., 2009]; Figure 1a) and from South Atlantic ODP Site 1090 (42°55'S, 8°54'E, 3702 m water depth [*Hodell et al*., 2003]; Figure 1a). These records have similar absolute values and G-IG amplitude to our record from Site 849, suggesting that $\delta^{13}C_b$ values recorded at Site 849 bear a high-latitude Southern Ocean signature (see Figure S9 in the supporting information). Crucially, our benthic and planktic foraminiferal $\delta^{13}C$ records from Site 849 show very similar trends to one another, lending support to the idea that our records are controlled by changes in the isotopic composition of the upwelled waters sourced in the high-latitude Southern Ocean from MIS G1 to 94, with minor G-IG fluctuations prior to MIS 100 and larger-scale G-IG changes from MIS 100 onward.

Contrary to the observed pattern of change in our SAR record, visual evaluation of Figures 7a–7d indicates that carbon isotope records do not lag $\delta^{18}O$. Hence, we infer that productivity at Site 849 as recorded by our SAR record was stimulated by changes in water mass properties (i.e., nutrient content) at the beginning of glacials MIS 100, 98, and 96 and further escalated toward terminations.

To conclude, the covariance as well as the constant offset observed between our $\delta^{13}C_{s,t}$ and $\delta^{13}C_b$ records from Site 849 can be explained when interpreting these records as tracers of Southern Ocean water mass

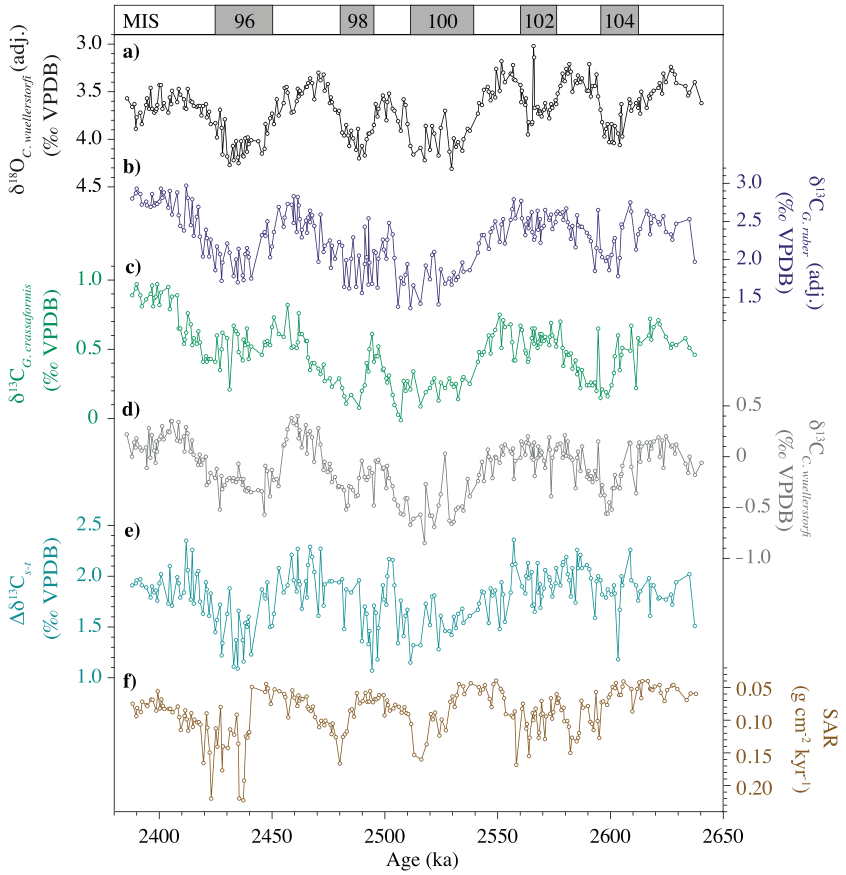

Figure 7. High-resolution foraminiferal $\delta^{13}C$ proxy records from Site 849. (a) Benthic foraminiferal (*C. wuellerstorfi*) $\delta^{18}O$ record. (b) $\delta^{13}C$ record of the sea surface-dwelling planktic foraminifera *G. ruber*. (c) $\delta^{13}C$ record of the subthermocline-dwelling planktic foraminifera *G. crassaformis*. (d) $\delta^{13}C$ record of the benthic foraminifera *C. wuellerstorfi*. (e) $\delta^{13}C$ gradient between *G. ruber* and *G. crassaformis*. (f) Sand accumulation rates (>63 μm). Unfortunately, there is a paucity of other paired benthic-planktic high-resolution $\delta^{13}C$ records from sites located in the EEP for the latest Pliocene/earliest Pleistocene with which to compare our new records from Site 849.

signatures. This observation lends strong support to the hypothesis that Plio-Pleistocene surface water properties in the EEP largely result from high-latitude forcing.

5.5. Evidence for Superimposed Strengthened Trade Wind-Induced Upwelling in the Equatorial Pacific During Glacial Terminations 100 Through 96

In light of our SAR record, it seems that productivity at Site 849 starts to increase during full glacial conditions in response to enhanced nutrient delivery from high southern latitudes (as evidenced by our $\delta^{13}C$ records) and culminates, toward glacial terminations, possibly in response to local intensification in upwelling. To test for the hypothesized influence of upwelling intensification on biological production at Site 849, we make use of vertical $\delta^{13}C$ gradients between sea surface (*G. ruber*, $\delta^{13}C_s$) and thermocline-dwelling (*G. crassaformis*, $\delta^{13}C_t$) foraminifera ($\Delta\delta^{13}C_{s-t}$). This gradient is a useful proxy to decipher changes in the depth of the thermocline [e.g., *Pierre et al.*, 2001], which in turn is related to upwelling intensity. In the case of increased upwelling strength, the thermocline shoals, resulting in lower $\Delta\delta^{13}C_{s-t}$.

Our $\Delta\delta^{13}C_{s-t}$ record (Figure 7e) shows relatively constant values prior to MIS 100, indicating that upwelling intensity was stable from ~2.64 to ~2.56 Ma. For the interval spanning MIS 100 to 96, however, a decrease in the $\Delta\delta^{13}C_{s-t}$ gradient of >1‰ occurred during glacials, reaching its minimum value toward glacial terminations (Figure 7e). This suggests a prominent shoaling of the thermocline probably in response to intensified regional upwelling during terminations, a mechanism which was activated from MIS 100 onward at least during the investigated time interval (see section 6.2).

6. Primary Productivity Variability in the Eastern Equatorial Pacific: A Response to Glacial-Interglacial Ice Sheet Dynamics?

Our results point to G-IG changes in export productivity in the equatorial Pacific Ocean during culmination of iNHG, controlled by nutrient supply from the Southern Ocean and superimposed wind-driven upwelling during MIS 100, 98, and 96. Next we explore potential mechanisms for these linkages that involve G-IG waxing and waning of the LIS and sea ice extent in the Southern Ocean.

The LIS and Southern Ocean sea ice coverage have the potential to affect the EEP upwelling system in at least two ways. First, G-IG changes in the size of the LIS are a main controlling factor for meridional pressure gradients that regulate trade wind intensity and equatorial upwelling strength [e.g., *Pisias and Mix*, 1997, and references therein; *Oster et al*., 2015]. Second, G-IG changes of Antarctic sea ice coverage control, through light limitation, the rate of biological production and thus the nutrient content in the Southern Ocean surface waters [e.g., *Nürnberg et al*., 1997; *Bonn et al*., 1998; *Hillenbrand and Cortese*, 2006]. Because Antarctic and sub-Antarctic surface waters are the major source for the upwelled water in the EEP [e.g., *Toggweiler et al*., 1991; *van de Flierdt et al*., 2004; *Sarmiento et al*., 2004], changes in the composition of this water mass may strongly influence the rate of primary productivity in the EEP upwelling system.

6.1. Strong Control of Primary Productivity in the Equatorial Pacific Upwelling System by Sea Ice Coverage in the Southern Ocean

One implication of our δ^{13}C-based interpretation of G-IG changes in nutrient supply to the equatorial Pacific is that Southern Ocean biological production was higher during interglacials than during glacials during iNHG [*Sigman et al*., 2004; *Hillenbrand and Cortese*, 2006], presumably because of reduced sea ice coverage [*Hillenbrand and Cortese*, 2006]. This picture is analogous to reconstructions of the late Pleistocene Southern Ocean [e.g., *Charles et al*., 1991; *Mortlock et al*., 1991]. At Site 849, high interglacial δ^{13}C signatures are seen in our records in response to the enhanced Southern Ocean biological production (Figure 8a). This suggestion gains support from the similarity between the $\delta^{13}C_b$ record from Site 849 and the $\delta^{13}C_b$ record from Site MV0502-4JC [*Waddell et al*., 2009], which is located within the pathway of AABW water mass advection from their high-latitude source area to the EEP (see section 5.4 and Figure S9). Through mixing of the AABW with SOW and upwelling to the sea surface at Site 849, this high interglacial δ^{13}C signature is also imprinted in planktic thermocline- and sea surface-dwelling foraminiferal tests as seen in our records (Figures 7b–7d). Moreover, reduced nutrient supply, resulting from the upwelling of relatively nutrient-depleted water masses sourced in the Southern Ocean, limits the biological production in the EEP during interglacials, as documented in our productivity records and in the paleoproductivity proxy data from Site 846 (Figure 5) [*Lawrence et al*., 2006; *Bolton et al*., 2010a].

The opposite signal is seen during glacials (Figure 8b) when biological production in the Southern Ocean is reduced compared to interglacials, probably because of light limitation in response to increased Antarctic sea ice cover as argued for late Pleistocene glacials [e.g., *Nürnberg et al*., 1997; *Bonn et al*., 1998; *Hillenbrand and Cortese*, 2006]. Reduced glacial primary productivity in the Southern Ocean results in less efficient use of nutrients and a slowdown of the biological pump, an observation that has also been recorded for the LGM [*Mortlock et al*., 1991]. In response to reduced phytoplankton activity, δ^{13}C in high-latitude sea surface waters decreases during glacials. The downwelled Southern Ocean surface waters bear this low glacial δ^{13}C signature and feed the AABW and the SOW and thus ultimately the upwelling system in the EEP [*Tsuchiya et al*., 1989; *Toggweiler et al*., 1991]. At Site 849, the inherited low glacial δ^{13}C signatures of the AABW and the SOW are recorded by benthic and planktic sea surface and thermocline-dwelling foraminifera, respectively (Figures 7b–7d). Furthermore, the enhanced glacial nutrient content of the source water leads to an increase in primary productivity within the EEP. This is documented by paleoproductivity records from Sites 849 (this study) and 846 (Figure 5) [*Lawrence et al*., 2006; *Bolton et al*., 2010a].

Our benthic and planktic foraminiferal δ^{13}C records indicate that nutrient delivery from high southern latitudes was active during the investigated time interval, but only with minor implications for G-IG primary productivity changes in the EEP prior to MIS 100 compared to the time interval from MIS 100 onward. We suggest

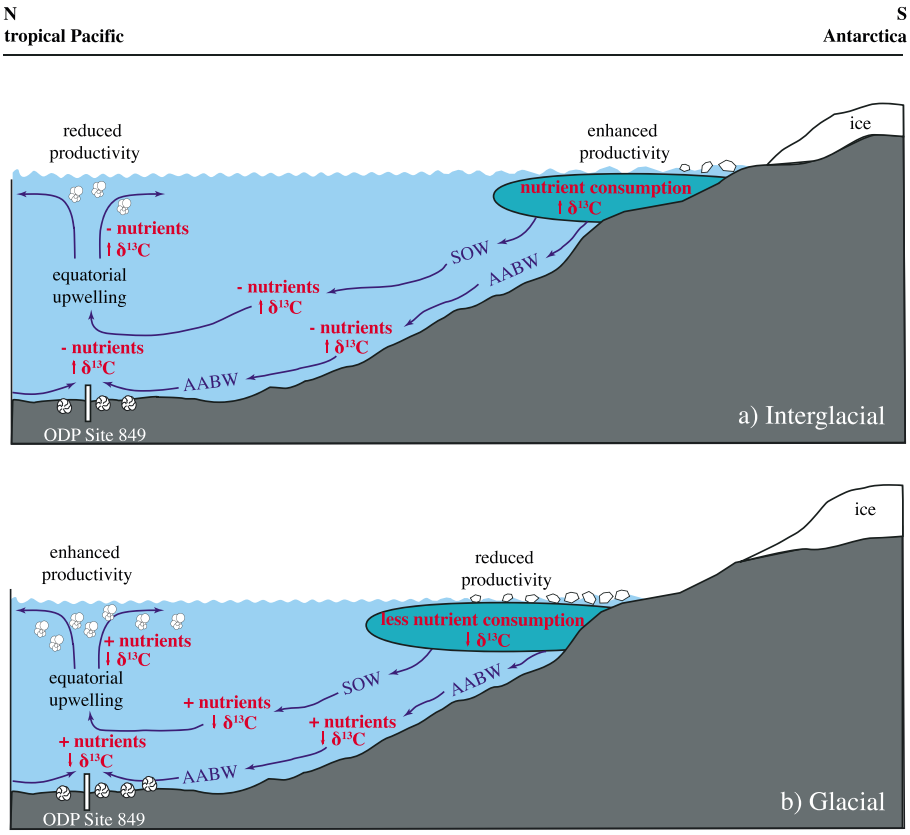

Figure 8. Schematic north-south section of the South Pacific Ocean from Antarctica/Southern Ocean to the EEP upwelling system. Primary productivity and resulting nutrient utilization and $\delta^{13}C$ signatures are proposed for early Pleistocene (a) interglacial and (b) glacial periods. AABW: Antarctic Bottom Water; SOW: Southern Ocean Water.

that this is a consequence of less significant changes in Antarctic sea ice extent during the relatively weak glacials MIS 102 and 104.

6.2. Superimposed Enhanced Upwelling During Glacial Terminations From MIS 100 Onward in Response to Retreat of the Laurentide Ice Sheet?

In addition to the enhanced glacial nutrient delivery from the Southern Ocean to the EEP upwelling regime, we suggest that the rate of wind-induced upwelling of nutrients at Site 849 significantly increased toward glacial terminations MIS 100, 98, and 96. As evidenced by decreasing $\Delta\delta^{13}C_{s\text{-}t}$ values (compare section 5.5 and Figure 7e), wind-driven upwelling intensification was active from MIS 100 onward at least during the investigated time interval. The timing of the onset of this behavior is unlikely to be a coincidence. Marine isotope stage 100 was the first glacial to result in ice rafting throughout the open North Atlantic Ocean [e.g., *Shackleton et al.*, 1984]. Its significance for the equatorial Pacific Ocean may lie in being the first glacial during which the LIS advanced into the midlatitudes of North America [*Naafs et al.*, 2013], something that perhaps did not occur again until ~1.3 Ma [*Balco and Rovey*, 2010]. Studies of the LGM suggest that a large LIS is associated with major changes in atmospheric circulation well beyond North America [e.g., *Oster et al.*, 2015]. The profile of the LIS during MIS 100 must have been lower slung than its late Pleistocene counterparts, probably in response to ready flow on soft nonpreglaciated substrates [*Clark and Pollard*, 1998; *Bailey et al.*, 2010], but LIS height and extent during iNHG and MIS 100 in particular had a major impact on hydroclimate, both over the ice sheet itself [*Bailey et al.*, 2010] and beyond the ice front in the midlatitudes [*Naafs et al.*, 2012; *Hennissen et al.*, 2014, 2015; *Lang et al.*, 2014] and perhaps into the arid North American southwest [*Lang et al.*, 2014].

Our data suggest enhanced glacial equatorial upwelling strength during our study interval from MIS 100 onward implying strengthened meridional pressure gradients and trade wind intensity. Export production (SAR), however, lags global ice volume (benthic $\delta^{18}O$) by ~9.5 kyr in our records (Figure 6). Similar observations

have been made for the past 1 Myr and for the LGM at central equatorial Pacific Sites PC72 [*Murray et al*., 2000] and U1338 [*Lyle and Baldauf*, 2015], EEP Site 849 [*Ma et al*., 2015], and northeast Pacific Site NH22P [*Ganeshram et al*., 2000; *Kienast et al*., 2002] (Figure 1a). Explanations for this lagged relationship are speculative. Suggestions include (i) upwelling intensification during glacial terminations [*Kienast et al*., 2002; *Hayes et al*., 2011] and/or (ii) deglacial nutrient supply from continental shelves either during sea level rise associated with glacial terminations ("glacial outwash" [*Ma et al*., 2015]) or during sea level fall associated with glacials [*Flores et al*., 2012], assuming a lag between cause (weathering on exposed shelves) and effect (nutrient delivery to the deep ocean) of 10–20 kyr ("shelf sediment offloading" [*Filippelli et al*., 2007; *Markovic et al*., 2015]). We do not favor nutrient input from continental shelves attributable to glacial outwash or shelf sediment offloading to explain the lag of productivity with respect to climate (benthic δ^{18}O) in our records. These mechanisms should give rise to a regional response affecting all EEP productivity records covering MIS 100 to 96. Yet productivity does not lag benthic δ^{18}O at Site 846 (Figure S6) [e.g., *Lawrence et al*., 2006; *Bolton et al*., 2010a; *Etourneau et al*., 2013]. Instead, we suggest that upwelling intensification during glacial terminations can be traced to strengthening of the eastern Pacific subtropical high-pressure system and northeasterly trade winds as the LIS retreated. Climate modeling experiments covering the past 18 kyr show major changes in wind, sea level pressure, and sea surface temperature pattern for reduced versus maximum North American ice sheet size [*Kutzbach and Ruddiman*, 1993; *Kutzbach et al*., 1993]. A strengthening of surface atmospheric circulation (including the eastern Pacific and Bermuda high-pressure systems) associated with ice sheet retreat is well documented in these atmospheric simulations coinciding with the last deglaciation [e.g., *COHMAP Members*, 1988; *Kutzbach et al*., 1993; *Bartlein et al*., 1998, and references therein]. Thus, we conclude that glacial terminations of the low slung slippery late Pliocene/early Pleistocene LIS [*Bailey et al*., 2010] influenced regional climate and upwelling in the EEP system in a manner analogous to the late Pleistocene.

7. Conclusions

We present new records from ODP Site 849 to test competing hypotheses for G-IG changes in productivity during Plio-Pleistocene iNHG (MIS G1–94, ~2.65–2.4 Ma). The most salient features of our study are as follows.

Primary productivity changes in the low-latitude Pacific Ocean follow the obliquity-dominated G-IG cyclicity but lag peak glacials by ~9.5 kyr at Site 849. Export productivity increased during early Pleistocene glacials and reached maximum values during the glacial terminations of MIS 100, 98, and 96.

We identify two processes that regulate the observed G-IG variability in primary productivity at Site 849. These processes are (i) nutrient delivery from the Southern Ocean to the EEP, which was a regulating factor from MIS G1 to 94 and was presumably controlled by sea ice extent in the Southern Ocean, and (ii) the intensity of trade wind-induced upwelling in the EEP, which played a major role in regulating EEP export productivity during MIS 100, 98, and 96 and which we hypothesize to be controlled by strengthening of the eastern Pacific subtropical high-pressure system and northeasterly trade winds in response to retreat of the LIS. We propose that an interplay between intensified upwelling strength and enhanced nutrient delivery from high southern latitudes increased primary productivity rates in the EEP during glacials from MIS 100 to 96.

Acknowledgments
The data associated with this paper are provided in the supporting information (Tables S1 to S3 and Data Set S1). This research used samples provided by the Ocean Drilling Program (ODP). ODP was sponsored by the U.S. National Science Foundation (NSF) and participating countries under the management of Joint Oceanographic Institutions (JOI), Inc. Sven Hofmann (University of Frankfurt) is thanked for his support in stable-isotope analyses. Hans-Peter Meyer and Alexander Varychef (University of Heidelberg) are thanked for SEM assistance. Discussions with Silke Voigt (University of Frankfurt) are acknowledged. Jani L. Biber is thanked for taking samples at the Gulf Coast Repository (GCR), Texas A&M University in College Station, Texas. We thank Phil Rumford and his colleagues at the GCR for their support during sampling. C.T.B acknowledges OSU-Institut Pythéas. Comments and suggestions by David Naafs and an anonymous reviewer are highly appreciated. Funding for this study was provided by the German Research Foundation (Deutsche Forschungsgemeinschaft, DFG, grants FR2544/2 and FR2544/6 to O.F. and PR651/15 to J.P.) and by the Natural Environmental Research Council (NERC, grant NE/F00141X/1 to P.A.W.).

References

Adelseck, C. G., and T. F. Anderson (1978), The late Pleistocene record of productivity fluctuations in the eastern equatorial Pacific Ocean, *Geology*, *6*, 388–391.

Bailey, I., C. T. Bolton, R. M. DeConto, D. Pollard, R. Schiebel, and P. A. Wilson (2010), A low threshold for North Atlantic ice rafting from "low-slung slippery" late Pliocene ice sheets, *Paleoceanography*, *25*, PA1212, doi:10.1029/2009PA001736.

Bailey, I., G. M. Hole, G. L. Foster, P. A. Wilson, C. D. Storey, C. N. Trueman, and M. E. Raymo (2013), An alternative suggestion for the Pliocene onset of major northern hemisphere glaciation based on the geochemical provenance of North Atlantic Ocean ice-rafted debris, *Quat. Sci. Rev.*, *75*, 181–194.

Balco, G., and C. W. Rovey (2010), Absolute chronology for major Pleistocene advances of the Laurentide Ice Sheet, *Geology*, *38*(9), 795–798.

Bartlein, P. J., K. H. Anderson, P. M. Anderson, M. E. Edwardsm, C. J. Mock, R. S. Thompson, R. S. Webb, T. Webb, and C. Whitlock (1998), Paleoclimate simulations for North America over the past 21,000 years: Features of the simulated climate and comparisons with paleoenvironmental data, *Quat. Sci. Rev.*, *17*, 549–585.

Bassinot, F. C., L. Beaufort, E. Vincent, L. D. Labeyrie, F. Rostek, P. J. Müller, X. Quidelleur, and Y. Lancelot (1994), Coarse fraction fluctuations in pelagic carbonate sediments from the tropical Indian Ocean: A 1500-kyr record of carbonate dissolution, *Paleoceanography*, *9*, 579–600, doi:10.1029/94PA00860.

Beaulieu, S. E. (2002), Accumulation and fate of phytodetritus on the seafloor, *Oceanogr. Mar. Biol.*, *40*, 171–232.

Berger, W. H., M.-C. Bonneau, and F. L. Parker (1982), Foraminifera on the deep-sea floor: Lysocline and dissolution rate, *Oceanol. Acta*, *5*, 249–258.

Berstad, I. M., H. P. Sejrup, D. Klitgaard-Kristensen, and H. Haflidason (2003), Variability in temperature and geometry of the Norwegian Current over the past 600 yr: Stable isotope and grain size evidence from the Norwegian margin, *J. Quat. Sci.*, *18*(7), 591–602.

Billups, K., J. E. T. Channell, and J. Zachos (2002), Late Oligocene to early Miocene geochronology and paleoceanography from the subantarctic South Atlantic, *Paleoceanography*, *17*(1), 1004, doi:10.1029/2000PA000568.

Bjerknes, J. (1969), Atmospheric teleconnections from the equatorial Pacific, *Mon. Weather Rev.*, *97*(3), 163–172.

Bolton, C. T., K. T. Lawrence, S. J. Gibbs, P. A. Wilson, L. C. Cleaveland, and T. D. Herbert (2010a), Glacial-interglacial productivity changes recorded by alkenones and microfossils in late Pliocene eastern equatorial Pacific and Atlantic upwelling zones, *Earth Planet. Sci. Lett.*, *295*(3–4), 401–411.

Bolton, C. T., P. A. Wilson, I. Bailey, O. Friedrich, C. J. Beer, J. Becker, S. Baranwal, and R. Schiebel (2010b), Millennial-scale climate variability in the subpolar North Atlantic Ocean during the late Pliocene, *Paleoceanography*, *25*, PA4218, doi:10.1029/2010PA001951.

Bolton, C. T., K. T. Lawrence, S. J. Gibbs, P. A. Wilson, and T. D. Herbert (2011), Biotic and geochemical evidence for a global latitudinal shift in ocean biogeochemistry and export productivity during the late Pliocene, *Earth Planet. Sci. Lett.*, *308*(1–2), 200–210.

Bonn, W. J., F. X. Gingele, H. Grobe, A. Mackensen, and D. K. Fütterer (1998), Paleoproductivity at the Antarctic continental margin: Opal and barium records for the last 400 ka, *Palaeogeogr. Palaeoclimatol. Palaeoecol.*, *139*(3–4), 195–211.

Charles, C. D., P. N. Froelich, M. A. Zibello, R. A. Matlock, and J. J. Morley (1991), Biogenic opal in Southern Ocean sediments over the last 450,000 years: Implications for surface water chemistry and circulation, *Paleoceanography*, *6*, 697–728, doi:10.1029/91PA02477.

Clark, P. U., and D. Pollard (1998), Origin of the Middle Pleistocene transition by ice sheet erosion of regolith, *Paleoceanography*, *13*, 1–9, doi:10.1029/97PA02660.

Cleaveland, L. C., and T. D. Herbert (2007), Coherent obliquity band and heterogeneous precession band responses in early Pleistocene tropical sea surface temperatures, *Paleoceanography*, *22*, PA2216, doi:10.1029/2006PA001370.

Coale, K. H., et al. (1996), A massive phytoplankton bloom induced by an ecosystem-scale iron fertilization experiment in the equatorial Pacific Ocean, *Nature*, *383*, 495–501.

COHMAP Members (1988), Climatic changes of the last 18,000 years: Observations and model simulations, *Science*, *241*(4869), 1043–1052.

Cramer, B. S., J. R. Toggweiler, J. D. Wright, M. E. Katz, and K. G. Miller (2009), Ocean overturning since the Late Cretaceous: Inferences from a new benthic foraminiferal isotope compilation, *Paleoceanography*, *24*, PA4216, doi:10.1029/2008PA001683.

Curry, W. B., and D. W. Oppo (2005), Glacial water mass geometry and the distribution of $\delta^{13}C$ of ΣCO_2 in the western Atlantic Ocean, *Paleoceanography*, *20*, PA1017, doi:10.1029/2004PA001021.

DeConto, R. M., D. Pollard, P. A. Wilson, H. Palike, C. H. Lear, and M. Pagani (2008), Thresholds for Cenozoic bipolar glaciation, *Nature*, *455*(7213), 652–656.

Dekens, P. S., A. C. Ravelo, and M. D. McCarthy (2007), Warm upwelling regions in the Pliocene warm period, *Paleoceanography*, *22*, PA3211, doi:10.1029/2006PA001394.

Diester-Haass, L., P. A. Meyers, and L. Vidal (2002), The late Miocene onset of high productivity in the Benguela Current upwelling system as part of a global pattern, *Mar. Geol.*, *180*, 87–103.

Eguchi, N. O., H. Kawahata, and A. Taira (1999), Seasonal response of planktonic foraminifera to surface ocean condition: Sediment trap results from the central North Pacific Ocean, *J. Oceanogr.*, *55*, 681–691.

Elderfield, H., M. Vautravers, and M. Cooper (2002), The relationship between shell size and Mg/Ca, Sr/Ca, $\delta^{18}O$, and $\delta^{13}C$ of species of planktonic foraminifera, *Geochem. Geophys. Geosyst.*, *3*(8), 1052, doi:10.1029/2001GC000194.

Etourneau, J., R. Schneider, T. Blanz, and P. Martinez (2010), Intensification of the Walker and Hadley atmospheric circulations during the Pliocene-Pleistocene climate transition, *Earth Planet. Sci. Lett.*, *297*(1–2), 103–110.

Etourneau, J., C. Ehlert, M. Frank, P. Martinez, and R. Schneider (2012), Contribution of changes in opal productivity and nutrient distribution in the coastal upwelling systems to Late Pliocene/Early Pleistocene climate cooling, *Clim. Past*, *8*(5), 1435–1445.

Etourneau, J., R. S. Robinson, P. Martinez, and R. Schneider (2013), Equatorial Pacific peak in biological production regulated by nutrient and upwelling during the late Pliocene/early Pleistocene cooling, *Biogeosciences*, *10*(8), 5663–5670.

Filippelli, G. M., J. C. Latimer, R. W. Murray, and J.-A. Flores (2007), Productivity records from the Southern Ocean and the equatorial Pacific Ocean: Testing the glacial shelf-nutrient hypothesis, *Deep Sea Res., Part II*, *54*(21–22), 2443–2452.

Flores, J. A., F. J. Sierro, and I. Raffi (1995), Evolution of the calcareous nannofossil assemblage as a response to the paleoceanographic changes in the eastern equatorial Pacific Ocean from 4 to 2 Ma (Leg 138, Sites 849 and 852), in *Proceedings of the Ocean Drilling Program, Sci. Results*, vol. 138, pp. 163–176, Ocean Drill. Program, College Station, Tex.

Flores, J. A., G. M. Filippelli, F. J. Sierro, and J. Latimer (2012), The "White Ocean" hypothesis: A late Pleistocene Southern Ocean governed by coccolithophores and driven by phosphorus, *Front. Microbiol.*, *3*, 233, doi:10.3389/fmicb.2012.00233.

Friedrich, O., R. Schiebel, P. A. Wilson, S. Weldeab, C. J. Beer, M. J. Cooper, and J. Fiebig (2012), Influence of test size, water depth, and ecology on Mg/Ca, Sr/Ca, $\delta^{18}O$ and $\delta^{13}C$ in nine modern species of planktic foraminifers, *Earth Planet. Sci. Lett.*, *319*, 133–145.

Ganeshram, R. S., T. F. Pedersen, S. E. Calvert, G. W. McNeill, and M. R. Fontugne (2000), Glacial-interglacial variability in denitrification in the world's oceans: Causes and consequence, *Paleoceanography*, *15*, 361–376, doi:10.1029/1999PA000422.

Garcia, H. E., R. A. Locarnini, T. P. Boyer, J. I. Antonov, O. K. Baranova, M. M. Zweng, J. R. Reagan, and D. R. Johnson (2014), in *World Ocean Atlas 2013, Dissolved Inorg. Nutr. (Phosphate, Nitrate, Silic.)*, 25 pp., vol. 4, edited by S. Levitus, U.S. Gov. Print. Off., Washington, D. C.

Gibbard, P. L., M. J. Head, and M. J. C. Walker (2010), Formal ratification of the Quaternary System/Period and the Pleistocene Series/Epoch with a base at 2.58 Ma, *J. Quat. Sci.*, *25*(2), 96–102.

Groeneveld, J., E. C. Hathorne, S. Steinke, H. DeBey, A. Mackensen, and R. Tiedemann (2014), Glacial induced closure of the Panamanian Gateway during Marine Isotope Stages (MIS) 95–100, *Earth Planet. Sci. Lett.*, *404*, 296–306.

Haug, G. H., D. M. Sigman, R. Tiedemann, T. F. Pedersen, and M. Sarnthein (1999), Onset of permanent stratification in the subarctic Pacific Ocean, *Nature*, *401*, 779–782.

Hayes, C. T., R. F. Anderson, and M. Q. Fleisher (2011), Opal accumulation rates in the equatorial Pacific and mechanisms of deglaciation, *Paleoceanography*, *26*, PA1207, doi:10.1029/2010PA002008.

Hennissen, J. A. I., M. J. Head, S. De Schepper, and J. Groeneveld (2014), Palynological evidence for a southward shift of the North Atlantic current at ~2.6 Ma during the intensification of late Cenozoic Northern Hemisphere glaciation, *Paleoceanography*, *29*, 564–580, doi:10.1002/2013PA002543.

Hennissen, J. A. I., M. J. Head, S. De Schepper, and J. Groeneveld (2015), Increased seasonality during the intensification of Northern Hemisphere glaciation at the Pliocene-Pleistocene boundary ~2.6 Ma, *Quat. Sci. Rev.*, *129*, 321–332.

Herguera, J. C., and W. H. Berger (1991), Paleoproductivity from benthic foraminifera abundance: Glacial to postglacial change in the west-equatorial Pacific, *Geology*, *19*, 1173–1176.

Hillenbrand, C.-D., and G. Cortese (2006), Polar stratification: A critical view from the Southern Ocean, *Palaeogeogr. Palaeoclimatol. Palaeoecol.*, *242*(3–4), 240–252.
Hillenbrand, C.-D., and D. K. Fütterer (2001), Neogene to Quaternary deposition of opal on the continental rise west of the Antarctic Peninsula, ODP Leg 178, Sites 1095, 1096 and 1101, in *Proceedings of the Ocean Drilling Program*, *Sci. Results*, vol. 178, pp. 1–33, Ocean Drill. Program, College Station, Tex. [Available at http://www-odp.tamu.edu/publications/178_sr/VOLUME/CHAPTERS/SR178_23.PDF.]
Hodell, D. A., K. A. Venz, C. D. Charles, and U. S. Ninnemann (2003), Pleistocene vertical carbon isotope and carbonate gradients in the South Atlantic sector of the Southern Ocean, *Geochem. Geophys. Geosyst.*, *4*(1), 1004, doi:10.1029/2002GC000367.
Holbourn, A., W. Kuhnt, M. Frank, and B. A. Haley (2013), Changes in Pacific Ocean circulation following the Miocene onset of permanent Antarctic ice cover, *Earth Planet. Sci. Lett.*, *365*, 38–50.
Hovan, S. A. (1995), Late Cenozoic atmospheric circulation intensity and climatic history recorded by eolian deposition in the eastern equatorial Pacific Ocean, Leg 138, in *Proceedings of the Ocean Drilling Program*, *Sci. Results*, vol. 138, pp. 615–625, Ocean Drill. Program, College Station, Tex.
Hovan, S. A. (2013), Grain-size variations, eolian material and accumulation rates in sediments from ODP Hole 138-849B, doi:10.1594/PANGAEA.807833.
Johnson, T. C. (1972), Ocean-floor erosion in the equatorial Pacific, *Geol. Soc. Am. Bull.*, *83*(10), 3121–3144.
Johnson, T. C., E. L. Hamilton, and W. H. Berger (1977), Physical properties of calcareous ooze: Control by dissolution at depth, *Mar. Geol.*, *24*, 259–277.
Kemle von Mücke, S., and H. Oberhänsli (1999), The distribution of living planktic foraminifera in relation to southeast Atlantic oceanography, in *Use of Proxies in Paleoceanography: Examples From the South Atlantic*, edited by G. Fischer and G. Wefer, pp. 91–115, Springer, Berlin.
Kienast, S. S., S. E. Calvert, and T. F. Pedersen (2002), Nitrogen isotope and productivity variations along the northeast Pacific margin over the last 120 kyr: Surface and subsurface paleoceanography, *Paleoceanography*, *17*(4), 1055, doi:10.1029/2001PA000650.
Kleiven, H. F., E. Jansen, T. Fronval, and T. M. Smith (2002), Intensification of Northern Hemisphere glaciations in the circum Atlantic region (3.5–2.4 Ma)—Ice-rafted detritus evidence, *Palaeogeogr. Palaeoclimatol. Palaeoecol.*, *184*, 213–223.
Kutzbach, J. E., and W. F. Ruddiman (1993), Model description, external forcing, and surface boundary conditions, in *Global Climates Since the Last Glacial Maximum*, edited by H. E. Wright Jr. et al., pp. 12–23, Univ. of Minnesota Press, Minneapolis.
Kutzbach, J. E., P. J. Guetter, P. J. Behling, and R. Selin (1993), Simulated climatic changes: Results of the COHMAP climate-model experiments, in *Global Climates Since the Last Glacial Maximum*, edited by H. E. Wright Jr. et al., pp. 24–93, Univ. of Minnesota Press, Minneapolis.
Lalicata, J. J., and D. W. Lea (2011), Pleistocene carbonate dissolution fluctuations in the eastern equatorial Pacific on glacial timescales: Evidence from ODP Hole 1241, *Mar. Micropaleontol.*, *79*(1–2), 41–51.
Lang, D. C., et al. (2014), The transition on North America from the warm humid Pliocene to the glaciated Quaternary traced by eolian dust deposition at a benchmark North Atlantic Ocean drill site, *Quat. Sci. Rev.*, *93*, 125–141.
Lawrence, K. T., Z. Liu, and T. D. Herbert (2006), Evolution of the eastern tropical Pacific through Plio-Pleistocene glaciation, *Science*, *312*, 79–83.
Lawrence, K. T., D. M. Sigman, T. D. Herbert, C. A. Riihimaki, C. T. Bolton, A. Martinez-Garcia, A. Rosell-Mele, and G. H. Haug (2013), Time-transgressive North Atlantic productivity changes upon Northern Hemisphere glaciation, *Paleoceanography*, *28*, 740–751, doi:10.1002/2013PA002546.
Le, J., and N. J. Shackleton (1992), Carbonate dissolution fluctuations in the western equatorial Pacific during the late Quaternary, *Paleoceanography*, *7*, 21–42, doi:10.1029/91PA02854.
Le, J., A. C. Mix, and N. J. Shackleton (1995), Late Quaternary paleoceanography in the eastern equatorial Pacific Ocean from planktonic foraminifers: A high-resolution record from Site 846, in *Proceedings of the Ocean Drilling Program*, *Sci. Results*, vol. 138, pp. 675–693, Ocean Drill. Program, College Station, Tex.
Lisiecki, L. E., and M. E. Raymo (2005), A Pliocene-Pleistocene stack of 57 globally distributed benthic δ^{18}O records, *Paleoceanography*, *20*, PA1003, doi:10.1029/2004PA001071.
Loubere, P. (2000), Marine control of biological production in the eastern equatorial Pacific Ocean, *Nature*, *406*, 497–500.
Lunt, D. J., G. L. Foster, A. M. Haywood, and E. J. Stone (2008), Late Pliocene Greenland glaciation controlled by a decline in atmospheric CO_2 levels, *Nature*, *454*(7208), 1102–1106.
Lyle, M., and J. Baldauf (2015), Biogenic sediment regimes in the Neogene equatorial Pacific, IODP Site U1338: Burial, production, and diatom community, *Palaeogeogr. Palaeoclimatol. Palaeoecol.*, *433*, 106–128.
Ma, Z., A. C. Ravelo, Z. Liu, L. Zhou, and A. Paytan (2015), Export production fluctuations in the eastern equatorial Pacific during the Pliocene-Pleistocene: Reconstruction using barite accumulation rates, *Paleoceanography*, *30*, 1455–1469, doi:10.1002/2015PA002860.
Mackensen, A., and T. Bickert (1999), Stable carbon isotopes in benthic foraminifera: Proxies for deep and bottom water circulation and new production, in *Use of Proxies in Paleoceanography: Examples From the South Atlantic*, edited by G. Fischer and G. Wefer, pp. 229–254, Springer, Berlin.
Mackensen, A., H.-W. Hubberten, T. Bickert, G. Fischer, and D. K. Fütterer (1993), The δ^{13}C in benthic foraminiferal tests of *Fontbotia wuellerstorfi* (Schwager) relative to the δ^{13}C of dissolved inorganic carbon in southern ocean deep water: Implications for glacial ocean circulation models, *Paleoceanography*, *8*, 587–610, doi:10.1029/93PA01291.
Mackensen, A., M. Rudolph, and G. Kuhn (2001), Late Pleistocene deep-water circulation in the sub-antarctic eastern Atlantic, *Global Planet. Change*, *30*, 197–229.
Marchitto, T. M., J. Lynch-Stieglitz, and S. R. Hemming (2005), Deep Pacific $CaCO_3$ compensation and glacial-interglacial atmospheric CO_2, *Earth Planet. Sci. Lett.*, *231*(3–4), 317–336.
Markovic, S., A. Paytan, and U. G. Wortmann (2015), Pleistocene sediment offloading and the global sulfur cycle, *Biogeosciences*, *12*, 3043–3060, doi:10.5194/bg-12-3043-2015.
Mayer, L., et al. (1985), *Proceedings of the Deep Sea Drilling Project*, *Initial Rep.*, vol. 85, Deep Sea Drill. Proj., Washington, D. C.
Mayer, L., et al. (1992), *Proceedings of the Ocean Drilling Program*, *Initial Rep.*, vol. 138, Ocean Drill. Program, College Station, Tex.
McGee, D., F. Marcantonio, and J. Lynch-Stieglitz (2007), Deglacial changes in dust flux in the eastern equatorial Pacific, *Earth Planet. Sci. Lett.*, *257*(1–2), 215–230.
Mix, A. C., N. G. Pisias, W. Rugh, J. Wilson, A. Morey, and T. K. Hagelberg (1995), Benthic foraminifer stable isotope record from Site 849 (0–5 Ma): Local and global climate changes, in *Proceedings of the Ocean Drilling Program*, *Sci. Results*, vol. 138, pp. 371–412, Ocean Drill. Program, College Station, Tex.
Mortlock, R. A., C. D. Charles, P. N. Froelich, M. A. Zibello, J. Saltzmann, J. D. Hays, and L. H. Burckle (1991), Evidence for lower productivity in the Antarctic Ocean during last glaciation, *Nature*, *351*, 220–223.
Murray, R. W., C. Knowlton, M. Leinen, A. C. Mix, and C. H. Polsky (2000), Export production and carbonate dissolution in the central equatorial Pacific Ocean over the past 1 Myr, *Paleoceanography*, *15*, 570–592, doi:10.1029/1999PA000457.

Naafs, B. D. A., J. Hefter, G. Acton, G. H. Haug, A. Martínez-Garcia, R. Pancost, and R. Stein (2012), Strengthening of North American dust sources during the late Pliocene (2.7 Ma), *Earth Planet. Sci. Lett.*, *317*, 8–19.

Naafs, B. D. A., J. Hefter, and R. Stein (2013), Millennial-scale ice rafting events and Hudson Strait Heinrich(-like) events during the late Pliocene and Pleistocene: A review, *Quat. Sci. Rev.*, *80*, 1–28, doi:10.1016/j.quascirev.2013.08.014.

Nakai, S., A. N. Halliday, and D. K. Rea (1993), Provenance of dust in the Pacific Ocean, *Earth Planet. Sci. Lett.*, *119*, 143–157.

Nürnberg, C. C., G. Bohrmann, and M. Schlüter (1997), Barium accumulation in the Atlantic sector of the Southern Ocean: Results from 190,000-year records, *Paleoceanography*, *12*, 594–603, doi:10.1029/97PA01130.

Oster, J. L., D. E. Ibarra, M. J. Winnick, and K. Maher (2015), Steering of westerly storms over western North America at the Last Glacial Maximum, *Nat. Geosci.*, *8*(3), 201–205.

Paillard, D., L. Labeyrie, and P. Yiou (1996), Macintosh program performs time-series analysis, *Eos Trans. AGU*, *77*(39), 379, doi:10.1029/1096EO00259.

Pälike, H., et al. (2012), A Cenozoic record of the equatorial Pacific carbonate compensation depth, *Nature*, *488*(7413), 609–614.

Paytan, A., M. Lyle, A. Mix, and Z. Chase (2004), Climatically driven changes in oceanic processes throughout the equatorial Pacific, *Paleoceanography*, *19*, PA4017, doi:10.1029/2004PA001024.

Pennington, J. T., K. L. Mahoney, V. S. Kuwahara, D. D. Kolber, R. Calienes, and F. P. Chavez (2006), Primary production in the eastern tropical Pacific: A review, *Prog. Oceanogr.*, *69*(2–4), 285–317.

Pichat, S., K. W. W. Sims, R. François, J. F. McManus, S. Brown Leger, and F. Albarède (2004), Lower export production during glacial periods in the equatorial Pacific derived from $(^{231}Pa/^{230}Th)_{xs,0}$ measurements in deep-sea sediments, *Paleoceanography*, *19*, PA4023, doi:10.1029/2003PA000994.

Pierre, C., J. F. Saliege, M. J. Urrutiaguer, and J. Giraudeau (2001), Stable isotope record of the last 500 k.y. at Site 1087 (Southern Cape Basin), in *Proceedings of the Ocean Drilling Program*, *Sci. Results*, vol. 175, pp. 1–22, Ocean Drill. Program, College Station, Tex., doi:10.2973/odp.proc.sr.175.230.2001.

Pisias, N. G., and A. C. Mix (1997), Spatial and temporal oceanographic variability of the eastern equatorial Pacific during the Late Pleistocene: Evidence from radiolaria microfossils, *Paleoceanography*, *12*, 381–393, doi:10.1029/97PA00583.

Pisias, N. G., L. A. Mayer, and A. C. Mix (1995), Paleoceanography of the eastern equatorial Pacific during the Neogene: Synthesis of Leg 138 drilling results, in *Proceedings of the Ocean Drilling Program*, *Sci. Results*, vol. 138, pp. 5–21, Ocean Drill. Program, College Station, Tex.

Poore, H. R., R. Samworth, N. J. White, S. M. Jones, and I. N. McCave (2006), Neogene overflow of Northern Component Water at the Greenland-Scotland Ridge, *Geochem. Geophys. Geosyst.*, *7*, Q06010, doi:10.1029/2005GC001085.

Pusz, A. E., R. C. Thunell, and K. G. Miller (2011), Deep water temperature, carbonate ion, and ice volume changes across the Eocene-Oligocene climate transition, *Paleoceanography*, *26*, PA2205, doi:10.1029/2010PA001950.

Ravelo, A. C., and R. G. Fairbanks (1992), Oxygen isotopic composition of multiple species of planktonic foraminifera: Recorders of the modern photic zone temperature gradient, *Paleoceanography*, *7*, 815–831, doi:10.1029/92PA02092.

Reynolds, L., and R. C. Thunell (1985), Seasonal succession of planktonic foraminifera in the subpolar North Pacific, *J. Foraminiferal Res.*, *15*, 282–301.

Saraswat, R. (2015), Non-destructive foraminiferal paleoclimatic proxies: A brief insight, *Proc. Indian Natl. Sci. Acad.*, *81*(2), 381–395.

Sarmiento, J. L., et al. (2004), Response of ocean ecosystems to climate warming, *Global Biogeochem. Cycles*, *18*, GB3003, doi:10.1029/2003GB002134.

Sarnthein, M., and J. Fenner (1988), Global wind-induced change of deep-sea sediment budgets, new ocean production and CO_2 reservoirs ca. 3.3–2.35 Ma BP, *Philos. Trans. R. Soc. London, Ser. A*, *318*, 487–504.

Sarnthein, M. K., K. Winn, J. C. Duplessy, and M. R. Fontugne (1988), Global variations of surface ocean productivity in low and mid-latitudes: Influence of CO_2, *Paleoceanography*, *3*, 361–399, doi:10.1029/PA003i003p00361.

Schlitzer, R. (2004), Export production in the equatorial and North Pacific derived from dissolved oxygen, nutrient and carbon data, *J. Oceanogr.*, *60*, 53–62.

Schneider, B., and A. Schmittner (2006), Simulating the impact of the Panamanian seaway closure on ocean circulation, marine productivity and nutrient cycling, *Earth Planet. Sci. Lett.*, *246*, 367–380.

Sepulchre, P., T. Arsouze, Y. Donnadieu, J.-C. Dutay, C. Jaramillo, J. Le Bras, E. Martin, C. Montes, and A. J. Waite (2014), Consequences of shoaling of the Central American Seaway determined from modeling Nd isotopes, *Paleoceanography*, *29*, 176–189, doi:10.1002/2013PA002501.

Sexton, P. F., and S. Barker (2012), Onset of "Pacific-style" deep-sea sedimentary carbonate cycles at the mid-Pleistocene transition, *Earth Planet. Sci. Lett.*, *321–322*, 81–94.

Sexton, P. F., P. A. Wilson, and P. N. Pearson (2006), Microstructural and geochemical perspectives on planktic foraminiferal preservation: "Glassy" versus "Frosty", *Geochem. Geophys. Geosyst.*, *7*, Q12P19, doi:10.1029/2006GC001291.

Shackleton, N. J., and M. A. Hall (1984), *Proceedings of the Deep Sea Drilling Project*, *Initial Rep.*, vol. 81, Deep Sea Drill. Proj., Washington, D. C.

Shackleton, N. J., J. Backman, H. Zimmerman, D. V. Kent, M. Hall, D. Roberts, D. Schnitker, J. Baldauf, A. Desprairies, and R. Homrighausen (1984), Oxygen isotope calibration of the onset of ice-rafting and history of glaciation in the North Atlantic region, *Nature*, *307*, 620–623.

Shackleton, N. J., M. A. Hall, and D. Pate (1995), Pliocene stable isotope stratigraphy of Site 846, in *Proceedings of the Ocean Drilling Program*, *Sci. Results*, vol. 138, pp. 337–355, Ocean Drill. Program, College Station, Tex.

Sigman, D. M., S. L. Jaccard, and G. H. Haug (2004), Polar ocean stratification in a cold climate, *Nature*, *428*, 59–63.

Spero, H. J., K. M. Mielke, E. M. Kalve, D. W. Lea, and D. K. Pak (2003), Multispecies approach to reconstructing eastern equatorial Pacific thermocline hydrography during the past 360 kyr, *Paleoceanography*, *18*(1), 1022, doi:10.1029/2002PA000814.

Stancin, A., J. Gleason, D. Rea, R. Owen, T. Moorejr, J. Blum, and S. Hovan (2006), Radiogenic isotopic mapping of late Cenozoic eolian and hemipelagic sediment distribution in the east-central Pacific, *Earth Planet. Sci. Lett.*, *248*(3–4), 840–850.

Steinke, S., H. Y. Chiu, P. S. Yu, C. C. Shen, L. Löwemark, H. S. Mii, and M. T. Chen (2005), Mg/Ca ratios of two *Globigerinoides ruber* (white) morphotypes: Implications for reconstructing past tropical/subtropical surface water conditions, *Geochem. Geophys. Geosyst.*, *6*, Q11005, doi:10.1029/2005GC000926.

Steph, S., R. Tiedemann, M. Prange, J. Groeneveld, M. Schulz, A. Timmermann, D. Nürnberg, C. Rühlemann, C. Saukel, and G. H. Haug (2010), Early Pliocene increase in thermohaline overturning: A precondition for the development of the modern equatorial Pacific cold tongue, *Paleoceanography*, *25*, PA2202, doi:10.1029/2008PA001645.

Takahashi, T., et al. (2009), Climatological mean and decadal change in surface ocean pCO_2, and net sea–air CO_2 flux over the global oceans, *Deep Sea Res., Part II*, *56*(8–10), 554–577.

Toggweiler, J. R., and J. L. Sarmiento (1985), Glacial to interglacial changes in atmospheric carbon dioxide: The role of ocean surface water in high latitudes, in *The Carbon Cycle and Atmospheric CO: Natural Variations Archean to Present*, *Geophys. Monogr. Ser.*, vol. 32, pp. 163–184, AGU, Washington, D. C.

Toggweiler, J. R., K. Dixon, and W. S. Broecker (1991), The Peru upwelling and the ventilation of the south Pacific thermocline, *J. Geophys. Res.*, *96*, 20,467–20,497, doi:10.1029/91JC02063.

Tsuchiya, M., R. Lukas, A. R. Fine, E. Firing, and E. J. Lindstrom (1989), Source waters of the Pacific equatorial undercurrent, *Prog. Oceanogr.*, *23*, 101–147.

van de Flierdt, T., M. Frank, D.-C. Lee, A. N. Halliday, B. C. Reynolds, and J. R. Hein (2004), New constraints on the sources and behavior of neodymium and hafnium in seawater from Pacific Ocean ferromanganese crusts, *Geochim. Cosmochim. Acta*, *68*(19), 3827–3843.

Waddell, L. M., I. L. Hendy, T. C. Moore, and M. W. Lyle (2009), Ventilation of the abyssal Southern Ocean during the late Neogene: A new perspective from the subantarctic Pacific, *Paleoceanography*, *24*, PA3206, doi:10.1029/2008PA001661.

Wang, L. (2000), Isotopic signals in two morphotypes of *Globigerinoides ruber* (white) from the South China Sea: Implications for monsoon climate change during the last glacial cycle, *Palaeogeogr. Palaeoclimatol. Palaeoecol.*, *161*, 381–394.

Watson, A. J., and A. C. N. Garabato (2006), The role of Southern Ocean mixing and upwelling in glacial-interglacial atmospheric CO_2 change, *Tellus, Ser. B*, *58*, 73–75.

Winckler, G., R. F. Anderson, M. Q. Fleisher, D. McGee, and N. Mahowald (2008), Covariant glacial-interglacial dust fluxes in the equatorial Pacific and Antarctica, *Science*, *320*, 93–96.

Wu, G., J. C. Herguera, and W. H. Berger (1990), Differential dissolution: Modification of late Pleistocene oxygen isotope records in the western equatorial Pacific, *Paleoceanography*, *5*, 581–594, doi:10.1029/PA005i004p00581.

Wyrtki, K. (1981), An estimate of equatorial upwelling in the Pacific, *J. Phys. Oceanogr.*, *11*, 1205–1214.

Zahn, R., K. Winn, and M. Sarnthein (1986), Benthic foraminiferal $\delta^{13}C$ and accumulation rates of organic carbon: *Uvigerina peregrina* group and *Cibicidoides wuellerstorfi*, *Paleoceanography*, *1*, 27–42, doi:10.1029/PA001i001p00027.

Ziegler, C. L., R. W. Murray, T. Plank, and S. R. Hemming (2008), Sources of Fe to the equatorial Pacific Ocean from the Holocene to Miocene, *Earth Planet. Sci. Lett.*, *270*(3–4), 258–270.